CIRP Annals - Manufacturing Technology 57 (2008) 81–84

Contents lists available at ScienceDirect

CIRP Annals - Manufacturing Technology

journal homepage: http://ees.elsevier.com/cirp/default.asp

An enhanced analytical model for residual stress prediction in machining

I. Lazoglu [a,*], D. Ulutan [b], B.E. Alaca [a], S. Engin [c], B. Kaftanoglu (1)[d]

[a] Department of Mechanical Engineering, Koc University, Istanbul, Turkey
[b] Ford Otosan Motor Company, Gebze Research Center, TUBITAK MAM, Kocaeli, Turkey
[c] Pratt & Whitney Canada Corporation, Department of Manufacturing Technology Development, Quebec, Canada
[d] Department of Mechnical Engineering, Middle East Technical University, Inonu Bulvari, 16531 Ankara, Turkey

ARTICLE INFO

Keywords:
Residual stresses
Simulation
Machining

ABSTRACT

The predictions of residual stresses are most critical on the machined aerospace components for the safety of the aircraft. In this paper, an enhanced analytic elasto-plastic model is presented using the superposition of thermal and mechanical stresses on the workpiece, followed by a relaxation procedure. Theoretical residual stress predictions are verified experimentally with X-ray diffraction measurements on the high strength engineering material of Waspaloy that is used critical parts such as in aircraft jet engines. With the enhanced analytical model, accurate residual stress results are achieved, while the computational time compared to equivalent FEM models is decreased from days to seconds.

1. Introduction

The major goal of this work is to develop a fast, accurate and an enhanced model for the predictions of the residual stresses on parts after machining processes. The predictions of residual stresses left on the part as a function of cutting conditions are critical to improve the fatigue life, fracture behavior, corrosion resistance and structural integrity of parts, especially in aerospace industry. There have been studies to predict and measure residual stresses in machining processes. Brinksmeier et al. [1] examined the effects of tool edge on residual stresses. Matsumoto et al. [2] experimentally investigated effects of cutting parameters on residual stresses in hard turning. Studies of residual stress modeling efforts are mostly on the FEM-based methods using rigid–plastic, elasto–plastic and elastic–viscoplastic models [3–6]. Although they perform well in general, FEM-based models require a long computation time, confined to parametric studies and are not rapidly applicable for machining process optimization in industry. Therefore, much faster and accurate analytical models are required for process optimization by industry [7,8].

The proposed analytical model considers combined isotropic and kinematic hardening for a better modeling of the inelastic deformation of the workpiece rather than isotropic hardening alone. Triangular distribution of mechanical forces was used instead of rectangular distribution in order to represent the contact physics closely. Contact length is calculated analytically using the contact load, radii and elastic modulus of the tool and the workpiece as opposed to approximating it as the half circle. Experimental cutting tests were performed on various machining conditions on Waspaloy and X-ray diffraction-based residual stress measurements are performed by the industrial collaborators in order to validate the analytical model. The residual stresses are predicted both in feed and crossfeed directions accurately in less than a minute.

2. Thermo-mechanical model

The schematic that describes the coordinate system used in thermo-mechanical model is shown in Fig. 1. There are distributed loads, p and q, in feed (z-direction) and tangential (x-direction) directions on the workpiece, respectively. Although easy to apply, the rectangular distribution does not represent the actual contact [7]. Hertzian contact is another frequently reported model in the literature; however, it is not easy to implement numerically, and it does not include tangential components of cutting forces. In this study, the loads are modeled as triangularly distributed forces. The magnitudes of the forces and temperature distribution are estimated from either measurements or predictions as explained in detail in [9–11].

As seen from Fig. 1, the system is considered to be two-dimensional. Representing the orthogonal cutting process, the problem geometry does not change along the out-of-plane direction. The workpiece is modeled as a semi-infinite material. The material is considered to be homogeneous, and it exhibits both isotropic and kinematic hardening. The temperature distribution serves as the source of thermal loading on the workpiece in addition to the mechanical loading.

2.1. Elastic loading

Workpiece has an elastic modulus, E; a Poisson's ratio, υ; coefficient of thermal expansion, α; isotropic hardening coefficient, h; and kinematic hardening coefficient, c. Plane strain condition is assumed on the workpiece, with ε_{yy}, the strain component in y-direction (out-of-plane direction), considered to

* Corresponding author.

0007-8506/$ – see front matter © 2008 CIRP.
doi:10.1016/j.cirp.2008.03.060

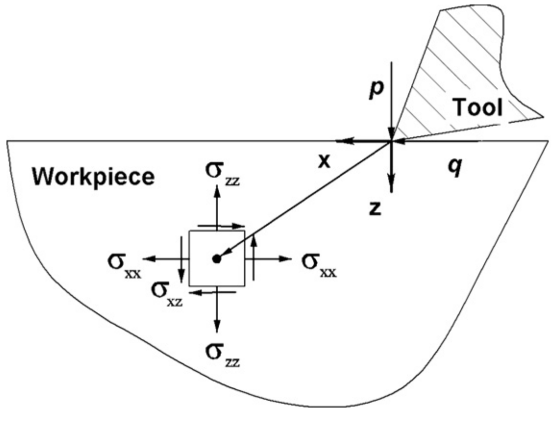

Fig. 1. Coordinate frame used in the model.

be zero. Therefore, the mechanical loading due to triangularly distributed forces in feed and tangential directions can be found by

$$\begin{aligned}\sigma_{xx}^{\text{mechanical}} &= -\frac{2z}{\pi}\int_{-a}^{a}\left(\frac{p(s)(x-s)^2+q(s)(x-s)^3}{((x-s)^2+z^2)^2}\right)\mathrm{d}s\\ \sigma_{zz}^{\text{mechanical}} &= -\frac{2z^3}{\pi}\int_{-a}^{a}\left(\frac{p(s)+q(s)(x-s)}{((x-s)^2+z^2)^2}\right)\mathrm{d}s\\ \sigma_{xz}^{\text{mechanical}} &= -\frac{2z^2}{\pi}\int_{-a}^{a}\left(\frac{p(s)(x-s)+q(s)(x-s)^2}{((x-s)^2+z^2)^2}\right)\mathrm{d}s\end{aligned} \tag{1}$$

where p is the normal force distribution (feed direction) and q is the tangential force distribution (cutting velocity direction) that are distributed as follows:

$$p(s) = f_\mathrm{f}\left(1-\frac{|s|}{a}\right), \quad q(s) = f_v\left(1-\frac{|s|}{a}\right) \tag{2}$$

x and z are the distances from the point of contact to the point of interest, s is the integration variable, f_v and f_f are the maximum magnitudes of the forces in cutting velocity and feed directions, respectively, and a is the half contact length, i.e. the contact takes place over $-a \le x \le a$. This contact length is a function of several parameters, and can be calculated from

$$a = \sqrt{\frac{4PR}{\pi E_\mathrm{R}}} \tag{3}$$

Here, P is the total normal force, R is the resultant radius of both the workpiece and the tool, and similarly, E_R is the resultant elastic modulus. These resultant values can be found by

$$\frac{1}{R} = \frac{1}{R_\mathrm{t}} + \frac{1}{R_\mathrm{w}}, \quad \frac{1}{E_\mathrm{R}} = \frac{1}{E_\mathrm{t}} + \frac{1}{E} \tag{4}$$

where R_t is the nose radius of the tool, R_w is the radius of the workpiece, and E_t is the elastic modulus of the tool. Since the radius of the workpiece is infinitely large compared to the nose radius of the tool, resultant radius can be taken as R_t.

The thermal loading due to the temperature field on the workpiece can be calculated by adding the following three stresses: (a) thermal stresses due to body forces, (b) thermal stresses due to surface traction, and (c) thermal stresses due to hydrostatic pressure.

Superposition of these three stresses will give the total thermal stresses, $\sigma_{ij}^{\text{thermal}}$, acting on the workpiece. The procedure was explained in detail in [7].

When the thermal and mechanical stresses are summed up, the total elastic stress components can be found at the point of interest for each tool position.

$$\begin{aligned}\sigma_m^{\text{elastic}} &= \sigma_m^{\text{mechanical}} + \sigma_m^{\text{thermal}}\\ \sigma_{yy}^{\text{elastic}} &= \upsilon(\sigma_{xx}^{\text{elastic}} + \sigma_{zz}^{\text{elastic}}) - \alpha E \Delta T\end{aligned} \tag{5}$$

where m represents the indices of xx, zz and xz. All other stress components are equal to zero. Here, ΔT is the temperature difference from room temperature.

Then, the deviatoric stresses are found by

$$S_{ij} = \sigma_{ij} - \tfrac{1}{3}\sigma_{kk}\delta_{ij} \tag{6}$$

The von Mises yield surface is defined by

$$f = \tfrac{1}{2}(S_{ij}-\alpha_{ij})(S_{ij}-\alpha_{ij}) - \tfrac{2}{3}\bar{\sigma}_0^2 = 0 \tag{7}$$

where $\bar{\sigma}_0$ is the current yield stress, and α_{ij} denoting the components of the deviatoric backstress. Combined isotropic and kinematic hardening is assumed, where both $\bar{\sigma}_0$ (isotropic part) and α_{ij} (kinematic part) are allowed to evolve.

In the elastic regime we have the following strain components:

$$\begin{aligned}\varepsilon_{xx}^{\text{elastic}} &= \frac{\sigma_{xx}}{E}(1-\upsilon^2) - \upsilon\frac{\sigma_{zz}}{E}(1+\upsilon) + \alpha\,\Delta T(1+\upsilon)\\ \varepsilon_{zz}^{\text{elastic}} &= \frac{\sigma_{zz}}{E}(1-\upsilon^2) - \upsilon\frac{\sigma_{xx}}{E}(1+\upsilon) + \alpha\,\Delta T(1+\upsilon)\\ \varepsilon_{yy}^{\text{elastic}} &= 0, \varepsilon_{xz}^{\text{elastic}} = \varepsilon_{zx}^{\text{elastic}} = \frac{\sigma_{xz}}{2G}\end{aligned} \tag{8}$$

2.2. Plastic loading

Fig. 1 depicts the discrete modeling of tool motion. The point of contact is slowly brought closer to the point of interest. With decreasing distance between the tool and the point of interest, stresses in Eq. (5) increase and at one point, the yield criterion in Eq. (7) is satisfied. It is then important to decrease the step size for the tool motion, since stress accumulation is now path-dependent.

Due to the similarities between the problem of machining and elasto-plastic rolling contact, the following stress invariant assumption is adopted [12]:

$$\sigma_{xx} = \sigma_{xx}^{\text{elastic}}, \quad \sigma_{zz} = \sigma_{zz}^{\text{elastic}}, \text{ and } \sigma_{xz} = \sigma_{xz}^{\text{elastic}}$$

σ_{yy} is then calculated by utilizing the plane strain assumption along the y direction.

Let us now address all contributions to ε_{yy}. Using the associated flow rule of plasticity, plastic strain increments can be written as

$$\mathrm{d}\varepsilon_{ij}^{\text{plastic}} = \frac{1}{h+c}\frac{3}{2\bar{\sigma}_0^2}(S_{kl}-\alpha_{kl})\,\mathrm{d}\sigma_{kl} \tag{9}$$

where h is the isotropic hardening coefficient and c is the kinematic hardening coefficient. Prager's rule is adopted for the evolution of backstresses, α_{ij}.

$\mathrm{d}\varepsilon_{yy}^{\text{plastic}}$ can be written specifically as follows:

$$\begin{aligned}&\mathrm{d}\varepsilon_{yy}^{\text{plastic}} = \frac{1}{h+c}\frac{3}{2\bar{\sigma}_0^2}(S_{yy}-\alpha_{yy}).\\ &(S_{xx}-\alpha_{xx})\,\mathrm{d}\sigma_{xx} + (S_{yy}-\alpha_{yy})\,\mathrm{d}\sigma_{yy} + (S_{zz}-\alpha_{zz})\,\mathrm{d}\sigma_{zz}\\ &\qquad + (S_{xz}-\alpha_{xz})\,\mathrm{d}\sigma_{xz} + (S_{zx}-\alpha_{zx})\,\mathrm{d}\sigma_{zx}\end{aligned} \tag{10}$$

The elastic and thermal strain increments can also be calculated as

$$\mathrm{d}\left(\varepsilon_{yy}^{\text{elastic}} + \varepsilon_{yy}^{\text{thermal}}\right) = \frac{\mathrm{d}\sigma_{yy}}{E} - \frac{\upsilon}{E}(\mathrm{d}\sigma_{xx} + \mathrm{d}\sigma_{zz}) + \alpha\,\Delta T \tag{11}$$

The sum of these stresses is then set to zero:

$$\mathrm{d}\varepsilon_{yy}^{\text{plastic}} + \mathrm{d}\varepsilon_{yy}^{\text{elastic}} + \mathrm{d}\varepsilon_{yy}^{\text{thermal}} = 0 \tag{12}$$

The coefficients of kinematic and isotropic hardening are found from the uniaxial loading–unloading data of the workpiece material.

Then, Eq. (12) is solved for $d\sigma_{yy}$, the differential stress increment in y-direction:

$$\begin{aligned}&\mathrm{d}\sigma_{yy} = \frac{(3/(h+c))((S_{yy}-\alpha_{yy})A/2\bar{\sigma}_0^2) + (\upsilon/E)(\mathrm{d}\sigma_{xx}+\mathrm{d}\sigma_{zz}) + \alpha\,\Delta T}{(1/E) + (1/(h+c))(3/(2\bar{\sigma}_0^2))(S_{yy}-\alpha_{yy})(S_{yy}-\alpha_{yy})}\\ &\text{where} \quad A = (S_{xx}-\alpha_{xx})\,\mathrm{d}\sigma_{xx} + (S_{zz}-\alpha_{zz})\,\mathrm{d}\sigma_{zz}\\ &\qquad\qquad + (S_{xz}-\alpha_{xz})\,\mathrm{d}\sigma_{xz} + (S_{zx}-\alpha_{zx})\,\mathrm{d}\sigma_{zx}\end{aligned} \tag{13}$$

After the computation of $\mathrm{d}\sigma_{yy}$, corresponding strain and back-stress increments are computed and $\bar{\sigma}_0$ is updated. Then the tool is moved by another increment and the procedure is repeated. If stresses start to decrease, elastic unloading is initiated, where Eq. (5) is again used to compute all stress increments.

2.3. Relaxation

When the unloading is complete, i.e. mechanical and thermal loading no longer exists (cutting forces are too far away and the temperature of the point of interest has decreased to ambient temperature), a certain distribution of stresses and strains is obtained. This distribution, however, does not correspond to the actual residual stress and strain distribution, σ^r_{ij} and ε^r_{ij}, respectively, due to the stress invariant assumption [12]. It is expected that,

(1) $\varepsilon^r_{xx} = 0$ (to ensure planarity of the surface after deformation), and
(2) $\sigma^r_{zz} = \sigma^r_{xz} = 0$ (to retain equilibrium and a traction-free surface).

Therefore, the following stress and strain increments are enforced:

$$\mathrm{d}\varepsilon_{xx} = -\frac{\varepsilon_{xx}}{M}, \mathrm{d}\sigma_{zz} = -\frac{\sigma_{zz}}{M} \text{ and } \mathrm{d}\sigma_{xz} = -\frac{\sigma_{xz}}{M} \tag{14}$$

After M steps, ε_{xx}, σ_{zz}, and σ_{xz} are reduced to zero. If the relaxation procedure is elastic, Hooke's Law is used to compute $\mathrm{d}\sigma_{xx}$ and $\mathrm{d}\sigma_{yy}$. If yielding occurs, then the following equations are solved simultaneously to determine $\mathrm{d}\sigma_{xx}$ and $\mathrm{d}\sigma_{yy}$:

$$\begin{aligned}
&\left\{\frac{3(S_{xx}-\alpha_{xx})(S_{yy}-\alpha_{yy})}{2\bar{\sigma}_0^2(h+c)} - \frac{\upsilon}{E}\right\}\mathrm{d}\sigma_{xx} \\
&\quad + \left\{\frac{3(S_{yy}-\alpha_{yy})(S_{yy}-\alpha_{yy})}{2\bar{\sigma}_0^2(h+c)} + \frac{1}{E}\right\}\mathrm{d}\sigma_{yy} \\
&\quad + \left\{\frac{3(S_{zz}-\alpha_{zz})(S_{yy}-\alpha_{yy})}{2\bar{\sigma}_0^2(h+c)} - \frac{\upsilon}{E}\right\}\mathrm{d}\sigma_{zz} \\
&\quad + \left\{\frac{3(S_{xz}-\alpha_{xz})(S_{yy}-\alpha_{yy})}{\bar{\sigma}_0^2(h+c)}\right\}\mathrm{d}\sigma_{xz} = 0, \\
&\left\{\frac{3(S_{xx}-\alpha_{xx})(S_{xx}-\alpha_{xx})}{2\bar{\sigma}_0^2(h+c)} + \frac{1}{E}\right\}\mathrm{d}\sigma_{xx} \\
&\quad + \left\{\frac{3(S_{yy}-\alpha_{yy})(S_{xx}-\alpha_{xx})}{2\bar{\sigma}_0^2(h+c)} - \frac{\upsilon}{E}\right\}\mathrm{d}\sigma_{yy} \\
&\quad + \left\{\frac{3(S_{zz}-\alpha_{zz})(S_{xx}-\alpha_{xx})}{2\bar{\sigma}_0^2(h+c)} - \frac{\upsilon}{E}\right\}\mathrm{d}\sigma_{zz} \\
&\quad + \left\{\frac{3(S_{xz}-\alpha_{xz})(S_{xx}-\alpha_{xx})}{\bar{\sigma}_0^2(h+c)}\right\}\mathrm{d}\sigma_{xz} = \mathrm{d}\varepsilon_{xx}
\end{aligned} \tag{15}$$

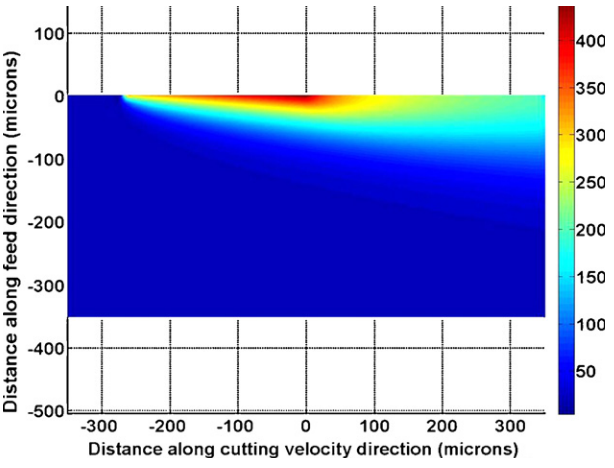

Fig. 2. Temperature field for the workpiece in °C for condition 2.

Table 1
Cutting conditions

	Condition		
	1	2	3
Cutting velocity (m/min)	54.9	25	54.9
Feed rate (mm/rev)	0.075	0.15	0.15
Tool rake angle (°)	0	5	0
Contact radius (μm)	34.1	51.6	39.2

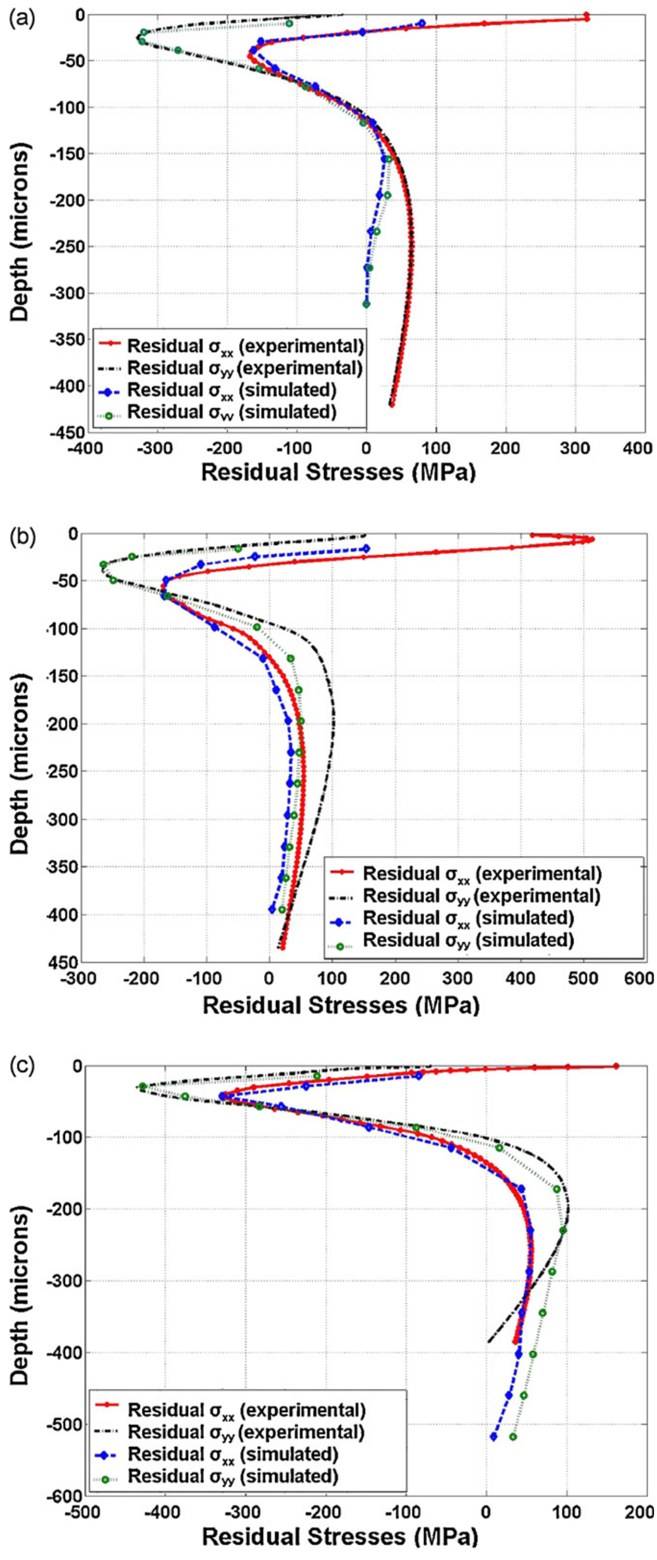

Fig. 3. Comparison of simulated and experimentally measured residual stresses for (a) condition 1, (b) condition 2 and for (c) condition 3.

At the end of the relaxation procedure, the resulting σ_{xx} and σ_{yy} are set equal to the corresponding residual stress components σ^r_{xx} and σ^r_{yy}, respectively.

3. Experimental validations

Experiments at various cutting conditions were performed on the advanced material Waspaloy. Sample results for three conditions are given in Table 1. The depth of cut was 0.25 mm and tool was Carbide VC29 with nose radius of 2.39 mm in all experiments. The tool had the elastic modulus (E_t) of 672 GPa. The properties of the workpiece material used in the tests and simulations are as follows; elastic modulus (E) of 210 GPa, plastic modulus (G) of 80.2 GPa, poisson's ratio (υ) of 0.314, initial yield strength ($\bar{\sigma}_0$) of 1016 MPa, isotropic hardening coefficient (h) of 500 MPa, kinematic hardening coefficient (c) of 1100 MPa, thermal expansion coefficient (α) of $0.15 \times 10^{-6}\,\mathrm{K}^{-1}$.

Residual stress measurements were carried out using X-ray diffraction technique in the depth of cut and cutting velocity directions. X-ray measurements were carried out using a sine-squared-psi technique in "iXRD Combo" X-ray diffraction machine. For the measurements, the radiation was Manganese K-alpha, which places the diffraction line of the (3 1 1) planes of the fcc lattice at about 155° (2-theta). The (3 1 1) family of planes offers a relatively high-intensity diffraction peak, in conjunction with a moderately high multiplicity factor mitigating the effects of preferred orientation and coarser grain size. For a typical measurement, 50 repetitions of a 0.8-s exposure were made with a 2-mm diameter X-ray beam at each of 9 beta tilt angles ranging from about −30° to +30°.

Temperature distributions in the tool, chip and workpiece were computed using previously developed finite difference-based thermal model [9,11]. Temperature distribution on the workpiece used in the residual stress calculations for condition 2 is given as an example in Fig. 2.

For validation purposes, analytical residual stress predictions are compared with the X-ray diffraction-based residual stress measurements for various conditions. Three of these comparisons (for the conditions given in Table 1) are given in Fig. 3.

It can be seen in the comparisons that residual stress simulation results both in the x and y directions are in very good agreement with the experimental residual stress measurements.

On and near the surface, tensile residual stresses, which may cause fracture initiations later on, are observed. Maximum tensile residual stress on the surface is around 500 MPa for condition 2. It is seen in these conditions compressive stresses take place up to subsurface depth of 150–200 μm, and maximum compressive residual stress occurs approximately between 20 and 60 μm beneath the machined surface. The maximum compressive stress may change from 150 to 450 MPa.

In these conditions, the residual stresses returns to zero level after 300 μm beneath the surface.

4. Conclusions

An analytical model is presented for predicting the residual stresses caused by the metal cutting process. The residual stress predictions are improved significantly, while reducing the computational time in comparison to finite element-based methods. The residual stress simulation and X-ray diffraction results on Waspaloy machining are presented. By changing the material properties and cutting conditions, the algorithm can be easily applied to different materials.

Since compressive surface residual stresses are often considered to be performance-enhancing in terms of fatigue life, stress state of the final product might be altered accordingly. Predicting the residual stresses fast and accurately allows the analytical model to be used as the potential tool for optimizing the process conditions.

Acknowledgments

The authors acknowledge the Scientific and Technical Research Council of Turkey (TUBITAK Project No. 104M287), Ministry of Industry and Trade (SANTEZ Project No. 00028.STZ.2007-1) and Pratt & Whitney Canada for their supports.

References

[1] Brinksmeier E, et al, (1982) Residual Stresses-Measurement and Causes in Machining Processes. *CIRP Annals* 31(2):491–510.
[2] Matsumoto Y, Hashimoto F, Lahoti G (1999) Surface Integrity Generated by Precision Hard Turning. *CIRP Annals* 48(1):59–62.
[3] Jacobus K, DeVor RE, Kapoor SG (2000) Machining-induced Residual Stress: Experimentation and Modeling. *Journal of Manufacturing Science and Engineering Transactions of ASME* 122:20–31.
[4] Chen L, El-Wardany TI, Harris WC (2004) Modeling the Effects of Flank Wear Land and Formation on Residual Stresses. *Annals of the CIRP* 53(1):95–98.
[5] Ee KC, Dillon OW, Jawahir IS (2005) Finite Element Modeling of Residual Stresses in Machining Induced by Cutting Using a Tool with Finite Edge Radius. *International Journal of Mechanical Sciences* 47:1611–1628.
[6] Outeiro JC, Umbrello D, Saoubi R (2006) Experimental and Numerical Modeling of the Residual Stresses Induced in Orthogonal Cutting of AISI 316L Steel. *International Journal of Machine Tools and Manufacture* 46:1786–1794.
[7] Ulutan D, Alaca BE, Lazoglu I (2007) Analytical Modeling of Residual Stresses in Machining. *Journal of Materials Processing Technology* 183:77–87.
[8] Liang SY, Su J-C (2007) Residual Stresses in Orthogonal Machining. *CIRP Annals* 56(1):65–68.
[9] Lazoglu I, Altintas Y (2002) Prediction of Tool and Chip Temperature in Continuous and Interrupted Machining. *International Journal of Machine Tools and Manufacture* 42:1011–1022.
[10] Lazoglu I, Kratz H, Buyukhatipoglu K, Klocke F (2006) Forces and Temperatures in Hard Turning. *Machining Science and Technology* 10(2):157–179.
[11] Dinc C, Lazoglu I, Serpenguzel A (2008) Analysis of Thermal Fields in Orthogonal Machining with Infrared Imaging. *Journal of Materials Processing Technology* 198:147–154.
[12] Jiang Y, Sehitoglu H (1994) An Analytical Approach to Elastic-Plastic Stress Analysis of Rolling Contact. *Journal of Tribology* 116:577–587.